



Effect of yttrium addition on microstructure, mechanical and corrosion properties of 20Cr13 martensitic stainless steel

Qi-yu Zang¹ · Yang-fan Jin¹ · Tuo Zhang¹ · Yi-tao Yang¹

Received: 11 January 2019 / Revised: 23 May 2019 / Accepted: 4 June 2019 / Published online: 18 March 2020
© China Iron and Steel Research Institute Group 2020

Abstract

The effects of rare-earth yttrium (Y) element on the microstructure, mechanical properties and corrosion properties of 20Cr13 martensitic stainless steel were investigated by optical microscopy, scanning electron microscopy and tensile test. Electrochemical experiments were carried out to study the effect of rare-earth element Y addition on corrosion resistance. The results showed that the addition of 0.02 wt.% rare-earth yttrium to martensitic stainless steel could affect the microstructure transformation, and A_{c3} temperature was obviously increased. In the stainless steel after heat treatment, there were more pro-eutectoid ferrite in the steel with 0.02 wt.% yttrium. The mechanical test results showed that the addition of 0.02 wt.% yttrium could significantly improve the tensile strength and elongation of the steel, which was related to the influence of yttrium element on inclusions in the test steel. With the quenching temperature of 0.02 wt.% yttrium steel increasing, the content of the ferrite in steel was affected and the corrosion resistance was remarkably improved.

Keywords Yttrium · Martensitic stainless steel · Mechanical property · Microstructural characterization · Corrosion resistance

1 Introduction

The hypoeutectoid 20Cr13 martensitic stainless steel is often used as a structural material for the manufacture of components with good mechanical properties and moderate corrosion resistance, such as the final stage of steam turbines, blades, fastening bolts, valve parts and the oil industry, because of its high corrosion resistance, impact resistance and temperature ductility [1–5]. However, there are still some problems in the application process. For example, the main failure of steam turbine blades is brittle fracture caused by vulcanized inclusions and stress corrosion [1]. Rare-earth elements have significant effects on the modification, deep purification, grain refinement and microalloying function of inclusions in alloy steel, improving mechanical properties and corrosion resistance [6–8].

In addition, the addition of rare-earth elements affects the phase transformation of the alloy steel, which also affects the properties of the steel. Yan et al. [9] studied the effect

of rare-earth addition on the austenitizing process of 30Mn steel. It was found that adding 0.2 wt.% rare earth to ferrosilicon alloy would increase the initial austenitization start temperature A_{c1} and final end temperature A_{c3} of 30Mn steel, producing a phase change activation and consequently increasing the relative content of ferrite and pearlite in the structure after cooling to room temperature.

In this study, the effect of yttrium addition on the microstructure, phase transformation, mechanical properties and corrosion resistance of 20Cr13 stainless steel was evaluated.

2 Experimental procedure

2.1 Materials and methods

In this experiment, the used ingots were obtained by smelting in a 25-kg vacuum induction furnace. The chemical composition of the stainless steel obtained by smelting is listed in Table 1. In order to reduce the segregation of the components, the alloys were first subjected to diffusion annealing at 1100 °C for 2 h and then austenitized at 1050 °C for 30 min, followed by water quenching. After quenching, they were tempered at 420 °C for 2 h and then air-cooled to room

✉ Yi-tao Yang
yangyitao@shu.edu.cn

¹ School of Materials Science and Engineering, Shanghai University, Shanghai 200444, China

Table 1 Chemical composition of investigated stainless steel (wt.%)

Steel	C	Si	Mn	S	Al	Ti	N	Cr	Y	Fe
0 Y	0.22	1.64	0.39	0.0176	0.0131	<0.0010	0.0244	12.75	–	Balance
0.02 wt.% Y	0.22	1.73	0.38	0.0076	0.0070	0.0055	0.0232	12.83	0.02	Balance

Table 2 Experimental parameters for studied samples

Sample	Y content/wt.%	Quenching temperature/°C
No. 1 steel	0	1050
No. 2 steel	0.02	1050
No. 3 steel	0.02	1080

temperature. The experimental sample with various Y additions after different heat treatments is shown in Table 2.

2.2 Microstructural investigation

Metallographical investigations were observed by optical microscopy (OM) and scanning electron microscopy (SEM, HITACHI SU-1500), while picric acid reagent was used as the etchant for microstructure observation.

2.3 Investigation of mechanical properties

Tensile test samples were cut in the size of the gage length and width of 25 mm and 6 mm, respectively. These samples were tested on an MTS tensile machine with a strain rate of 1 mm/min at room temperature.

2.4 Corrosion investigation

The heat-treated blocks were cut into corrosion samples with dimensions of 10 mm × 10 mm × 3 mm. The samples were ground successively to 1200 grit using water proof abrasive papers, and then these samples were mechanically polished and cleaned to obtain a fine surface. 3.5 wt.% NaCl aqueous solution was prepared by dissolving analytically pure NaCl in distilled water as the corrosion medium.

The electrochemical measurements were carried out using a standard electrochemical workstation (Gamry Reference 600) with a three-electrode cell, containing a saturated calomel electrode (SCE) as reference electrode, and the sample was prepared using the above method as the working electrode (WE). Before the electrochemical impedance spectroscopy (EIS) and polarization measurements were taken, the open-circuit potentials (OCPs) were monitored until a stable OCP was achieved. After a stable OCP was acquired, EIS measurements were performed with a frequency range from 10^5 to 10^{-2} Hz. The potentiodynamic polarization

measurements were conducted at a scanning rate of 1 mV/s from – 300 mV up to 600 mV with respect to OCP.

3 Results and discussion

3.1 Microstructure and principle analysis

The metallographic structure of different samples is presented in Fig. 1. Figure 1a shows the structure of martensitic laths and packets of experimental steel without Y under a quenching temperature of 1050 °C (No. 1 steel), and a small amount of other phases can also be observed. When the austenitizing temperature of experimental steel with 0.02 wt.% Y is 1050 °C (No. 2 steel), the structure is shown in Fig. 1b. In addition to the martensite lath, there are more other phases in the structure. The microhardness test was carried out and it was found that the microhardness of this phase was much lower than that of the martensite structure, and it was judged to be ferrite. When the quenching temperature of Y-containing sample was raised to 1080 °C (No. 3 steel, Fig. 1c), ferrite was still observed in the microstructure, but the content of ferrite was significantly reduced. It is indicated that the addition of 0.02 wt.% Y to the experimental steel will cause the appearance of pro-eutectoid ferrite, but the proportion of ferrite phase can be reduced by increasing the austenitizing temperature.

In order to further analyze the cause of the appearance of the ferrite phase, the phase transition of steel with 0 and 0.02 wt.% Y was tested, and the results are shown in Fig. 2. It can be seen from Fig. 2 that A_{c3} of steel with 0.02 wt.% Y is slightly higher than that without Y, indicating that the temperature of complete austenitization is increased by the addition of Y. When the quenching temperature of 1050 °C is close to that of A_{c3} (No. 2 steel), the phenomenon of incomplete austenitization occurs during austenitizing, so that the quenching temperature of 1080 °C for steel with Y (No. 3 steel) was also added. Zhang et al. [10] showed that with the increase in rare-earth content in steel, the phase transition starting point shifted to the left, that is, the incubation period of pro-eutectoid ferrite was shortened. Liu et al. [11] determined the critical point and continuous cooling transformation (CCT) curve of 20Mn steel by dilatometer. As the content of rare-earth increased, the points of A_{c1} , A_{c3} and A_{r3} are increased gradually, and the phase transition curve also gradually shifts to the left and moves upward.

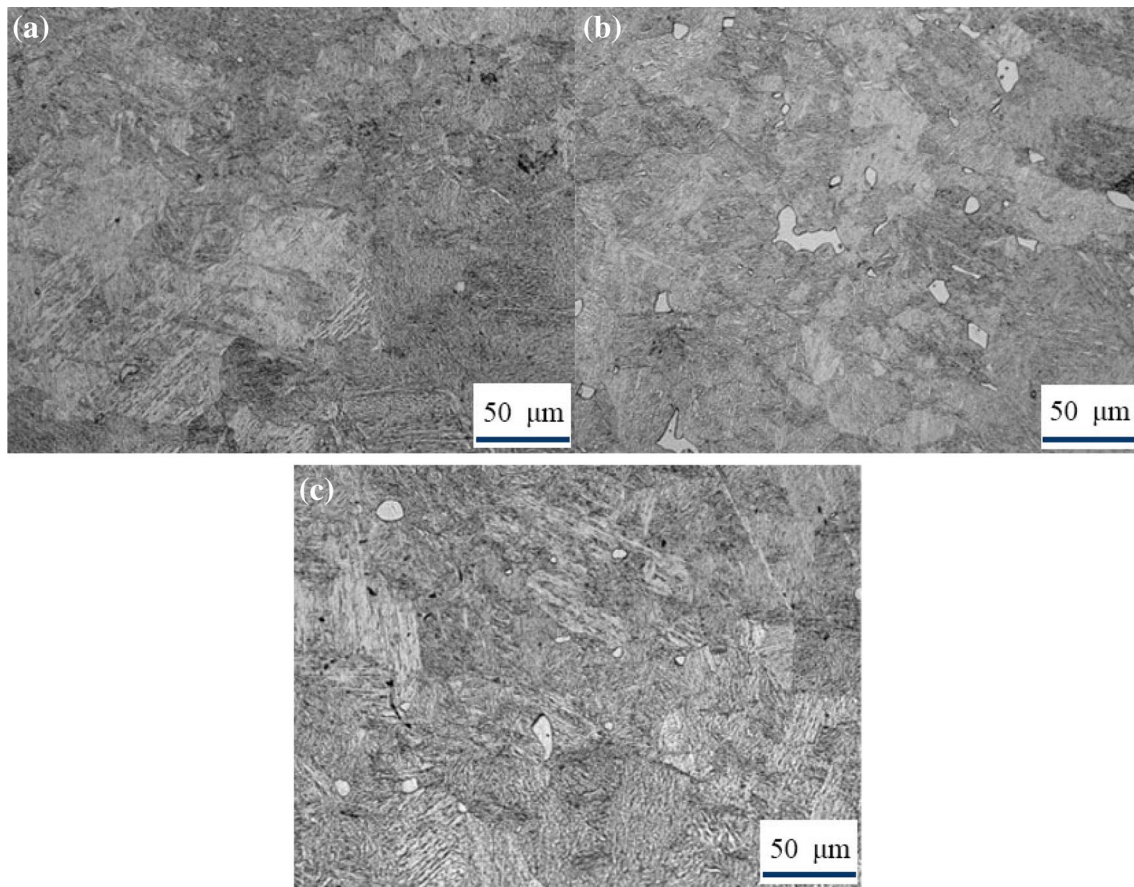


Fig. 1 Optical microstructure of No. 1 (a), 2 (b) and 3 (c) steels

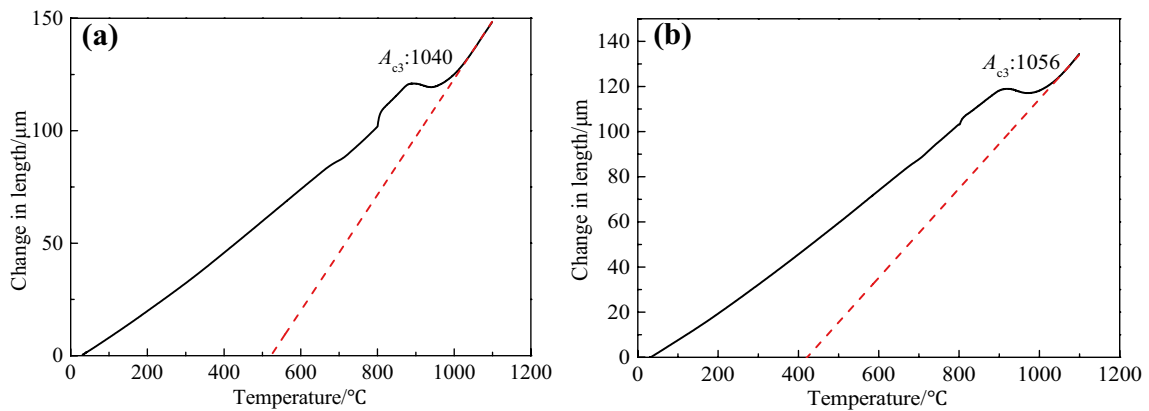


Fig. 2 Temperature rise curve of different samples. **a** 0 Y; **b** 0.02 wt.% Y

Lu et al. [12] studied the isothermal transformation curve of 0.27C-1Cr steel. It was found that the addition of rare earth could refine the austenite grains size, increase the nucleation rate and increase the total phase transition rate

of pro-eutectoid ferrite. A_{c3} phase transition point of 0.27C-1Cr steel was increased by 10 °C for the addition of rare earth. In this case, after the addition of Y for test steel, A_{c3} shifts by 16 °C and a higher temperature is required to

complete the austenitization. After the steel is heated to the austenitizing temperature (high temperature), the rare-earth elements enter the austenite and are mostly segregated at the grain boundaries, which influences the decomposition and transformation of supercooled austenite and also affects the content of ferrite.

Figure 3 presents SEM image of the microstructure of the samples with different Y contents. Figure 3a shows the microstructure of No. 1 steel, where the tissue species are mainly martensite, containing a small amount of ferrite phases (dark phase). No. 2 steel presents the martensite lath with ferrite phase (larger block darker phase), which is consistent with the result of Fig. 1, and confirms the ferrite phase (Fig. 3b). The precipitation of pro-eutectoid ferrite is a process of nucleation and growth. The nucleus of the pro-eutectoid ferrite is formed at the austenite grain boundary. The amount of precipitated pro-eutectoid ferrite depends on the carbon content of austenite and the precipitation temperature (or cooling rate). In the case of equilibrium cooling, the equiaxed pro-eutectoid ferrite first precipitates in

the steel, and the carbon atoms leave the ferrite and enter the austenite. When the austenite reaches the eutectoid component, it will transform to pearlite [13]. From the above discussion, the rare earth moves the decomposition kinetic curve of supercooled austenite to the left, shortening the incubation time of the pro-eutectoid ferrite (moves TTT curve or CCT curve to the left). Rare earth also has effect on raising A_{c3} , which is beneficial to the formation of pro-eutectoid ferrite.

The analysis results of inclusions and precipitates in No. 1 steel are given in Figs. 4 and 5. Figure 4 shows the bulky Al-, Ca- and O-rich inclusions in No. 1 steel. As shown in Fig. 5a, white granular precipitates (point A) and inclusion with a nearly spherical cross section (point B) are clearly presented. The energy spectrum analysis for the points is also performed in Fig. 5b, c, where point A represents carbide, and the near-spherical inclusions at point B are manganese sulfide (MnS).

Figure 6 presents SEM images of No. 2 steel with the corresponding energy-dispersive X-ray spectroscopy (EDS)

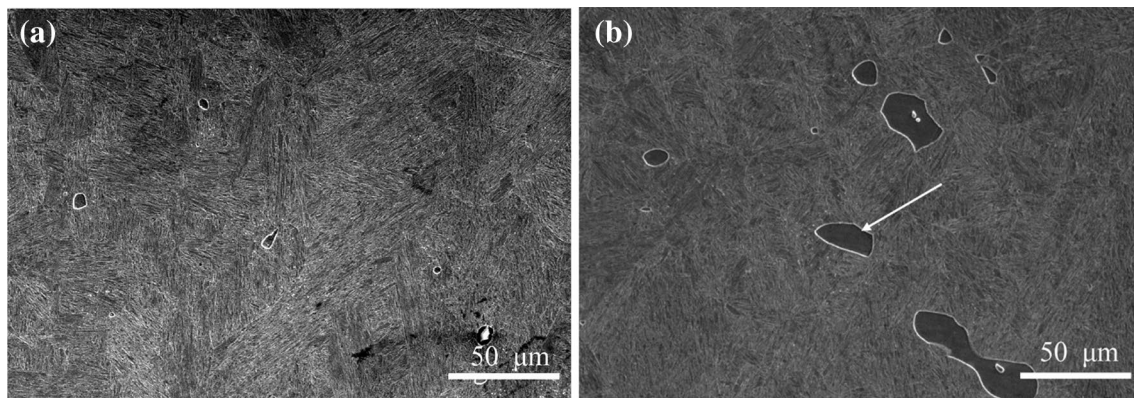


Fig. 3 SEM morphology of different samples. **a** No. 1 steel; **b** No. 2 steel

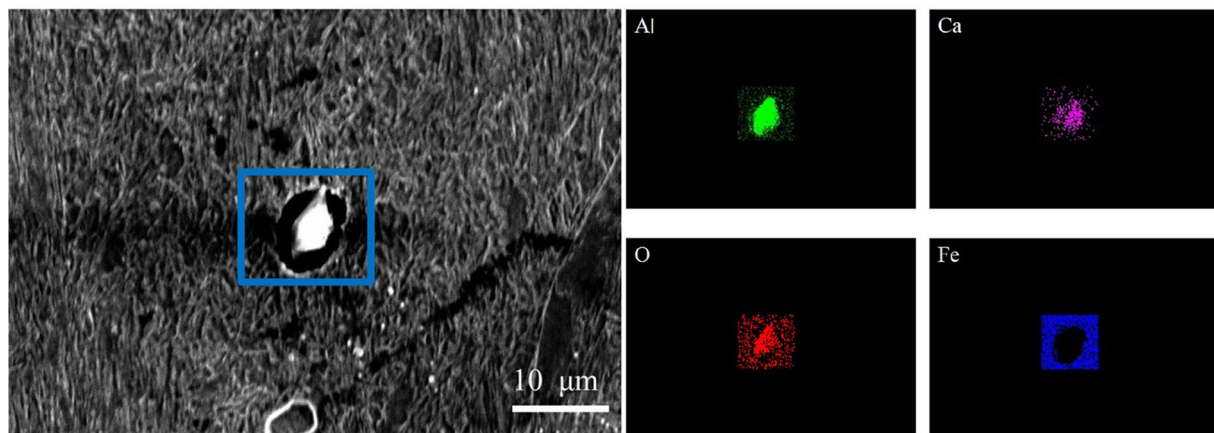


Fig. 4 Scanning analysis of inclusion surface of No. 1 steel

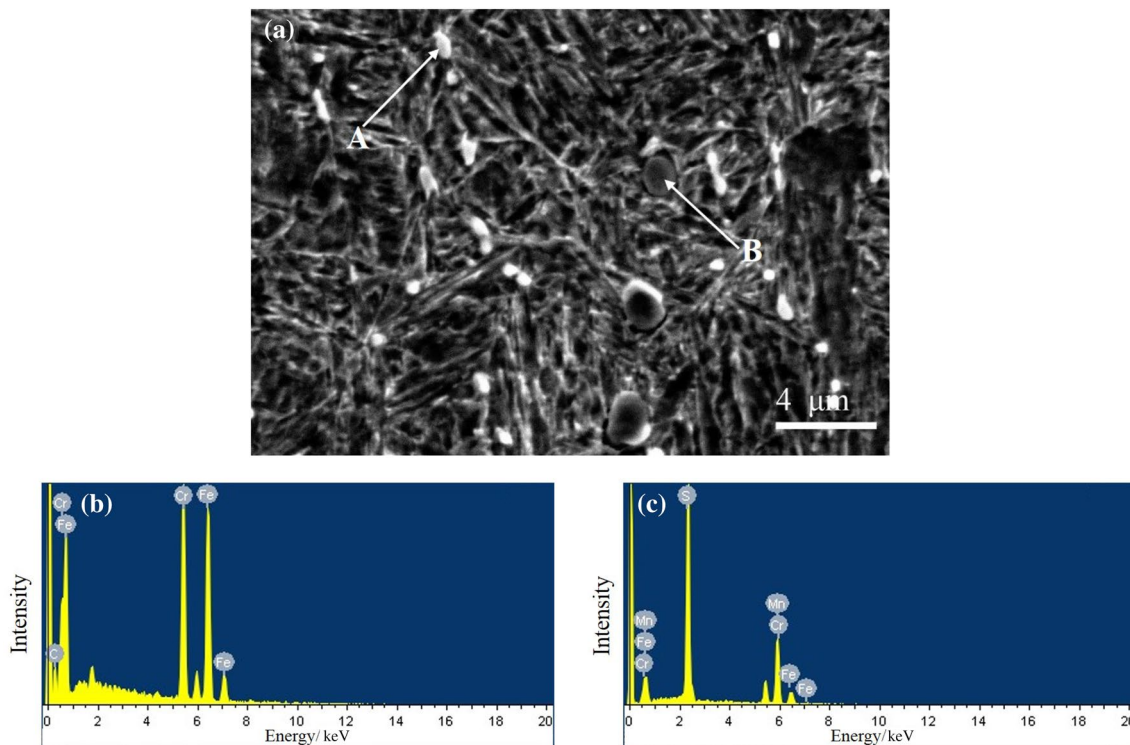
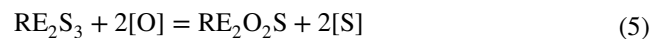
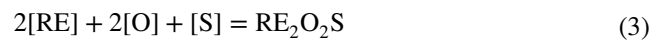


Fig. 5 Scanning and energy spectrum analysis of sulfide and carbide of No. 1 steel

spectrum analysis. The white particles appear at the center or boundary of the ferrite precipitated in the dark color, and they contain Y, Al, S, O or Ti and S by energy spectrum analysis (Fig. 6a–d). It can be judged that the white particles are inclusions, and the inclusions have a certain relationship with the formation of ferrite. EDS spectrum analysis was carried out on the white precipitated phase in the structure (Fig. 6e, f), and the carbide phase was found.

It can be seen that the larger particles of Al and O precipitates and the small particles of MnS inclusions appear in 20Cr13 martensitic stainless steel without Y, and the inclusions in 20Cr13 martensitic stainless steel mainly appear as small particles containing Y, Al, S, O, Ti or S when 0.02 wt.% Y element is added and quenching temperature is kept the same (Figs. 4–6). This indicates that addition of Y element to 20Cr13 martensitic stainless steel can purify the molten steel and desulfurize. After the rare-earth element is added to the steel, the rare earth can take the place of oxygen and sulfur in the inclusion of manganese sulfide, as well as alumina and aluminosilicate in the steel to form rare-earth composite inclusions; these inclusions can rise from the molten steel, and finally the steel is purified. Gao et al. [14] showed that addition of rare-earth elements to 20Cr13 martensitic stainless steel could form rare-earth inclusions, which reduced the distribution of inclusions in steel and purified molten steel. In general, the rare-earth desulfurization method is as follows [15]:



In Ref. [16], the solution systems of Fe–S–RE, Fe–O–RE and Fe–S–O–RE were studied from the viewpoint of thermodynamics, and it was found that rare-earth sulfur oxides were generally formed in iron liquids inevitably containing aerobic and sulfur. In general, rare-earth elements are first deoxidized in the molten iron, and then rare-earth sulfur oxides are formed. When the amount of [O] is reduced to a certain extent, there is a distinct single desulfurization product.

3.2 Mechanical properties

The stress–strain curves obtained for Nos. 1 and 2 steels under the same heat treatment condition are shown in Fig. 7. It can be seen from the stress–strain curves that the tensile strength and elongation of Y-containing steel are higher

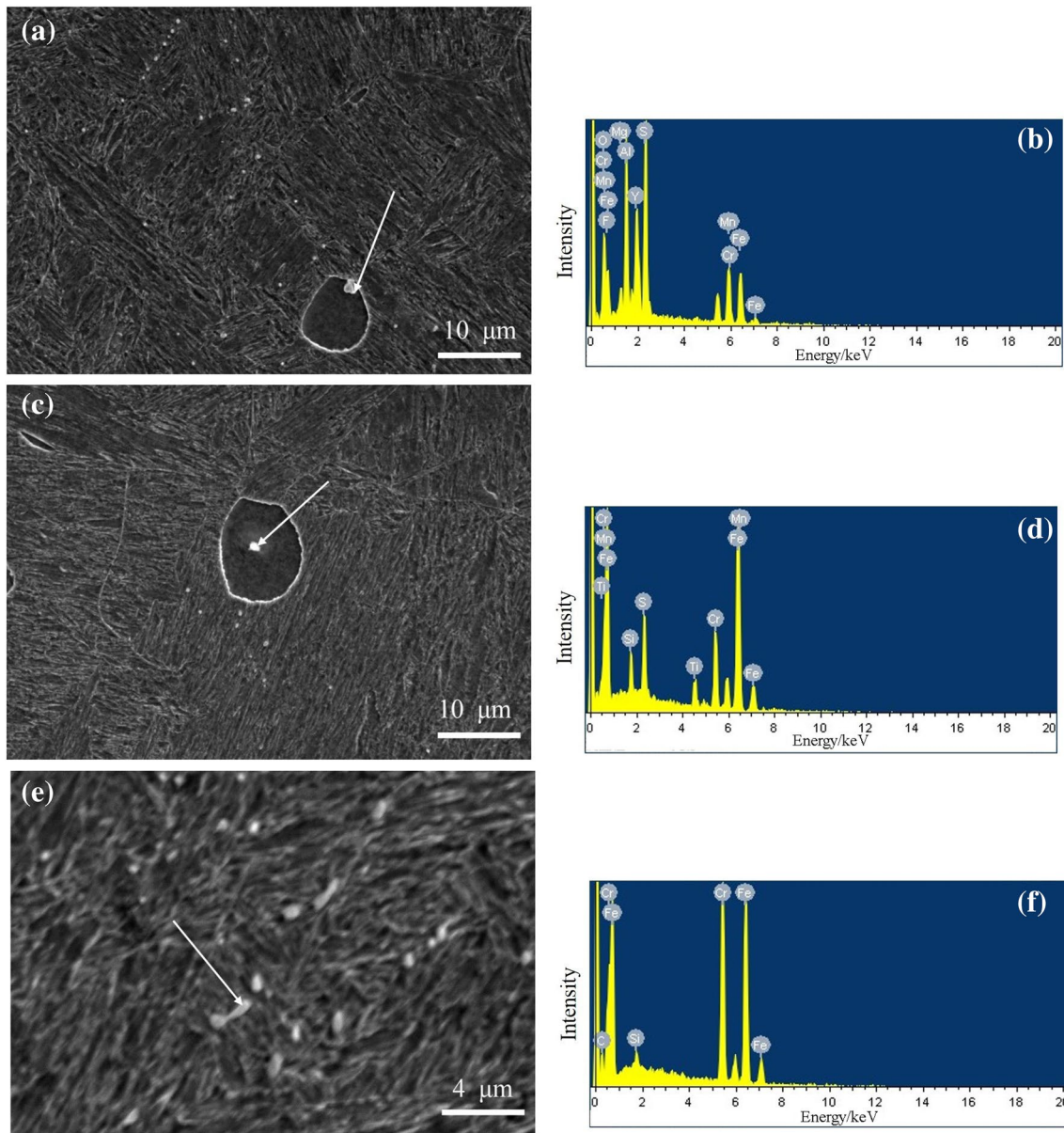


Fig. 6 Scanning and energy spectrum analysis of inclusions and carbides of No. 2 steel

than those without Y, with higher value of tensile strength (+ 330 MPa) for Y-containing steel than that without Y. Figure 8 shows SEM images of fracture surface of samples after tensile tests. Obvious dimples and tearing ribs can be seen from Fig. 8a, c. Figure 8b shows that strip-shaped MnS particles can also be found in the fractured dimples for steel without Y. Adding rare-earth Y to the austenitic heat-resistant stainless steel can affect the distribution of inclusions and the mechanical properties of the experimental steel at normal temperature and high temperature [17]. In addition, it has been reported that adding rare-earth elements to steel can play an important role in the purification of inclusions, improve the structure and have significant optimization

effect on the mechanical properties of steels [7, 8]. Small rare-earth metal-based inclusions have lower activity in crack initiation and crack propagation. In this study, the addition of rare-earth Y element can play a significant role in desulfurization and modifying inclusions. The remaining inclusions in steel are more diffusely distributed and smaller in size, and these smaller inclusions play a catalytic role in the improvement of strength and plasticity.

3.3 Corrosion properties

Figure 9 shows the potentiodynamic polarization curves of three samples. All the samples present a passivation region

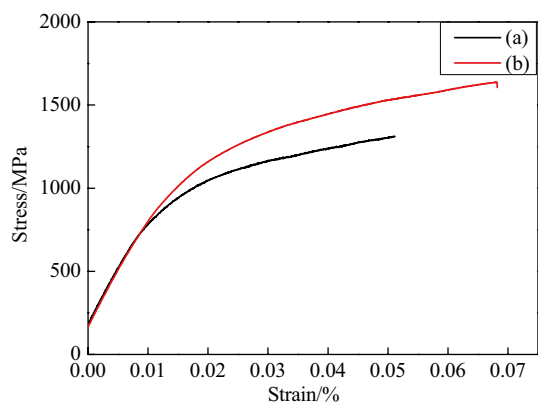


Fig. 7 Stress and strain curves of No. 1 steel (a) and No. 2 steel (b)

followed by pitting initiation, and all the passivation platforms appear obviously. The current density remains constant as the voltage increases, indicating that different samples have similar corrosion kinetics. For No. 1 and No. 3 steels, there is a significant current transient change in the passivation region of the corresponding polarization curves. After the applied voltage exceeding the passivation region,

the current density increased rapidly, which indicates the pitting situation. In this experiment, the potential at which the current density reached 0.1 mA/cm^2 is considered as pitting potential (E_{pit}), while higher pitting potential means better corrosion resistance. The corrosion potential (E_{corr}) was obtained by Tafel fitting on the polarization curve, and the fitting results are shown in Table 3. It can be seen from Table 3 that E_{corr} and E_{pit} of No. 3 steel are the highest, those of No. 1 steel are the second, and those of No. 2 steel are the lowest. If the heat treatment is suitable, addition of Y element could improve corrosion resistance of 20Cr13 martensitic stainless steel.

The impedance results for the three samples are presented in Fig. 10. Figure 10a shows the Nyquist diagram in EIS test. Z is represented for impedance. Z is an imaginary number, combined with real part (Z_{re}) and imaginary part (Z_{im}). The capacitive reactance arc during EIS test is related to the electric double-layer capacitance and the passivation film capacitance at the material/solution interface. The capacitive reactance arc of No. 2 steel is the smallest, and that of No. 3 steel is slightly larger than that of No. 1 steel, indicating that corrosion resistance of No. 3 steel is the best. In Fig. 10b, No. 3 steel has the highest impedance value, and No. 2 steels

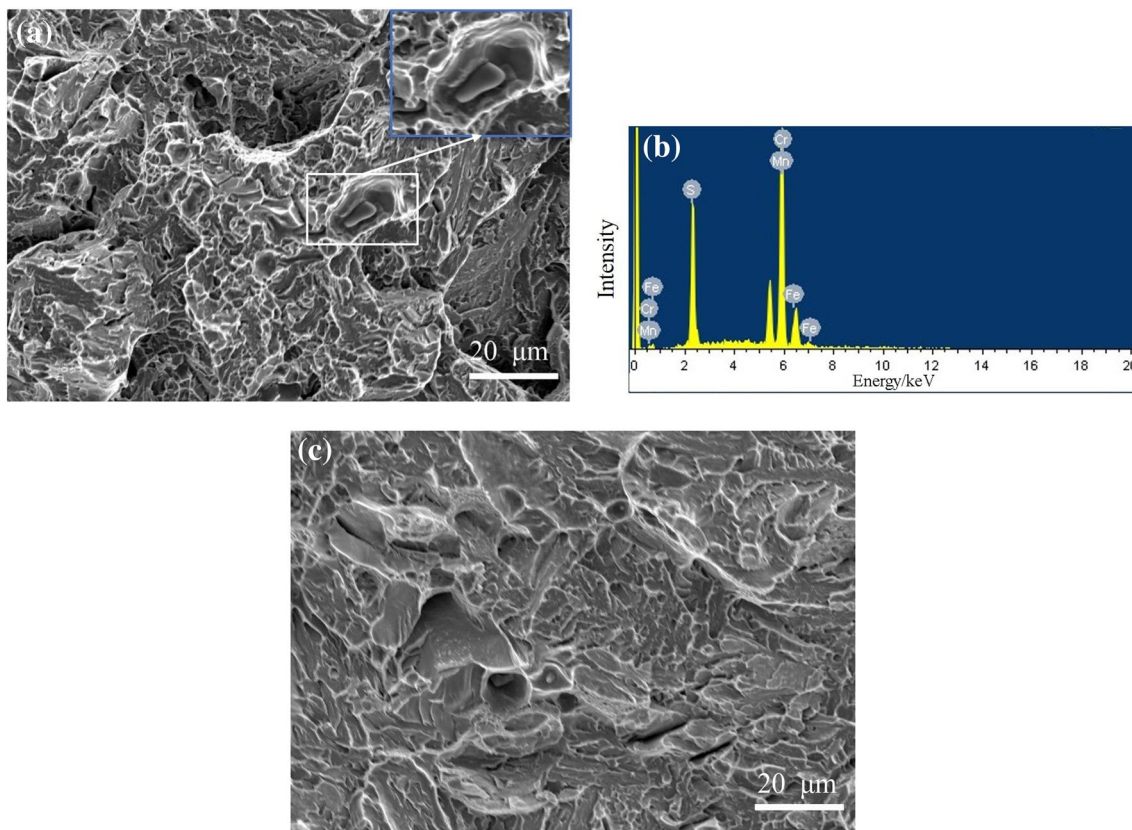


Fig. 8 Analysis of tensile fracture morphology and fracture inclusions. **a** Fracture morphology of No. 1 steel; **b** EDS of inclusion in frame of **a**; **c** fracture morphology of No. 2 steel

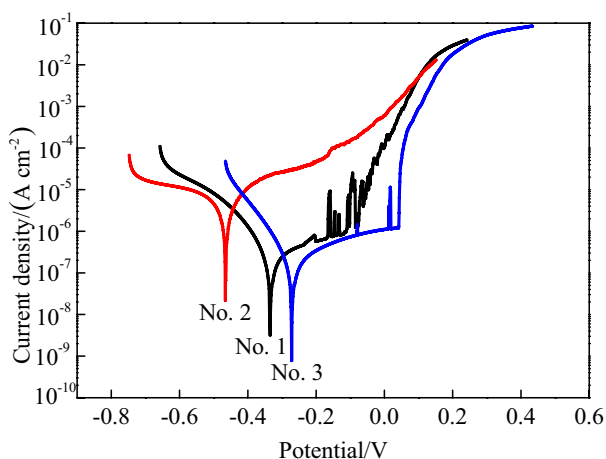


Fig. 9 Potentiodynamic polarization curves of different samples in 3.5 wt.% NaCl solution

Table 3 Dynamic potential scan results of different experimental samples

Sample	$E_{\text{corr}}/\text{mV}$	E_{pit}/mV
No. 1	-335	-9.97
No. 2	-466	-148.20
No. 3	-271	55.96

is the lowest, which is consistent with the Nyquist plot. Figure 10c shows a relatively flat auxiliary angle peak in the Bode diagram. It also represents that there is capacitive reactance in all test samples. It can also be found that No. 3 steel has the largest phase angle, and No. 2 steel has the smallest. The result is consistent with the Nyquist diagram.

In the actual research process, constant phase element (CPE) is often used as equivalent element of the electric double layer and the passivation film. Referred to the equivalent circuit model used for martensitic stainless steel [18, 19], the single $R(QR)$ equivalent circuit can be used to fit the electrochemical performance of the test samples. The equivalent circuit is shown in Fig. 11, in which the parallel resistance is CPE and the charge transfer resistance R_{ct} and the solution resistance R_s are in series with the parallel circuit. The impedance expression of CPE (Z_{CPE}) is as follows:

$$Z_{\text{CPE}} = Q_0^{-1} (j\omega)^{-\alpha} \quad (6)$$

where Q_0 is the original parameter of constant phase angle; the value of j is $\sqrt{-1}$; ω is the angular frequency; and α represents the diffusion coefficient related to surface non-uniformity.

According to Eq. (6), the fitting results are given in Table 4. It can be seen that α values of three samples range from 0.80 to 0.87, indicating that the performance of the passivation film of the three samples is affected by the surface uniformity. The data in Table 4 show that No. 3 steel has the highest value of R_{ct} and the relatively low value of Q_0 , indicating that the passivation film produced is the best, and thus No. 3 steel has the best corrosion resistance. Similarly, it can be analyzed that the performance of the passivation film of No. 2 steel is the worst.

It can be seen from the above results (Figs. 9, 10 and Tables 3, 4) that the corrosion resistance of No. 3 steel is the best, while that of No. 2 steel is the worst. Some scholars [20–22] indicated that the addition of rare-earth elements could form rare-earth composite inclusions and reduce the formation of sulfides, oxides and sulfur–oxygen composite oxides in duplex steels. The interface area between the object and the substrate is reduced, causing the reduction in pitting preferential formation position, which will improve the pitting corrosion resistance of the experimental steel. In this experiment, the addition of Y element has a purifying effect and deterioration effect on the sulfide of 20Cr13 martensitic stainless steel (as shown in Figs. 4–6), which improves the corrosion resistance of stainless steel with Y element. However, it can be seen from the electrochemical test results that the corrosion resistance of No. 2 steel is lower than that of No. 1 steel, with equal quenching condition of 1050 °C. This may be explained by the fact that the addition of 0.02 wt.% Y element in the experimental steel produced the large irregularly shaped ferrite phase in martensite matrix (Fig. 1 or Fig. 3), indicating that 0.02 wt.% Y steel was not completely austenitized at 1050 °C (No. 2 steel), and the ferrite phase was responsible for poor corrosion resistance of 20Cr13 martensitic stainless steel.

After the austenitizing temperature was raised to 1080 °C, ferrite structure still appears in No. 3 steel, but the proportion of ferrite phase is relatively small, and finally corrosion resistance of steel is significantly improved.

4 Conclusions

1. The addition of Y element causes a large ferrite structure to appear in 20Cr13 martensitic stainless steel. This is related to the influence of rare-earth elements on the phase transformation of experimental steel. Also, Y element leads to the increase in A_{c3} temperature from 1040 to 1056 °C (+16 °C) compared to the steel without Y.
2. The addition of Y element can improve the tensile strength and plasticity of 20Cr13 martensitic stainless steel, which is related to the deterioration and purifica-

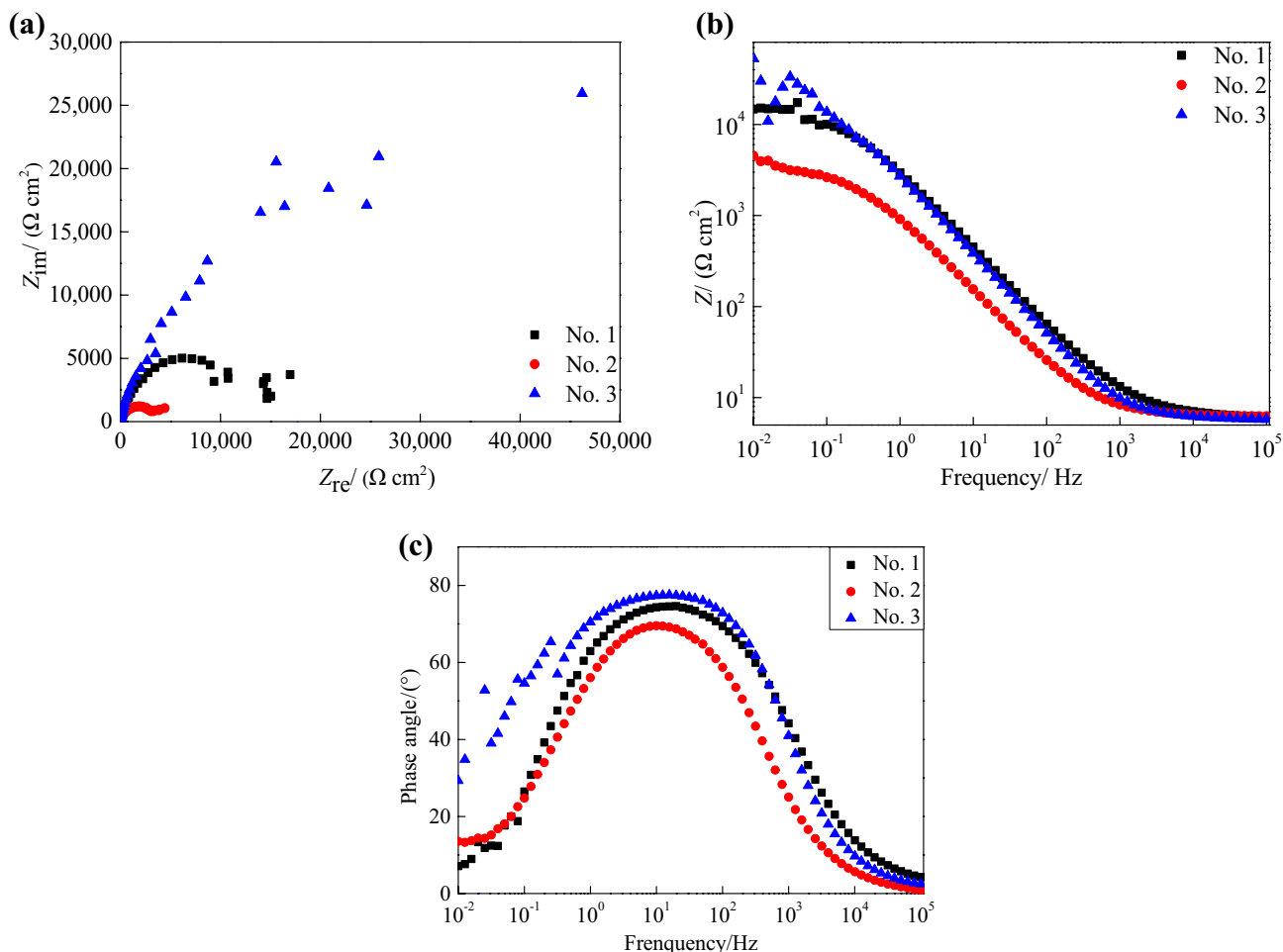


Fig. 10 EIS spectrum of different samples in 3.5 wt.% NaCl aqueous solution. **a** Nyquist plot; **b** impedance-frequency plot; **c** bode phase angle plot

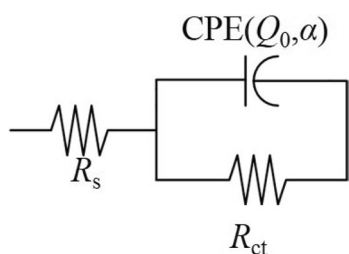


Fig. 11 EIS fitting equivalent circuit diagram, and this kind of equivalent circuit can be written as $R(QR)$

Table 4 EIS fitting parameters

Samples	$R_s/(\Omega \text{ cm}^2)$	CPE		$R_{ct}/(\text{k}\Omega \text{ cm}^2)$
		α	$Q_0/(\text{M}\Omega^{-1} \text{ cm}^{-2} \text{ s}^\alpha)$	
No. 1	6.399	0.8353	70.15	14.43
No. 2	6.316	0.8041	234.10	3.60
No. 3	5.918	0.8663	75.22	19.60

tion effect of element Y on oxides and sulfides in test steel.

- The corrosion resistance of 20Cr13 martensitic stainless steel with Y element is not only affected by the deterioration and purification of inclusions but also the morphology and quantity of ferrite in the structure. Quench-

ing at 1080 °C can significantly improve the corrosion resistance of No. 3 steel.

References

[1] X. Liu, J.C. Yang, L. Yang, X.Z. Gao, J. Iron Steel Res. Int. 17 (2010) No. 12, 59–64.

- [2] S.X. Li, P.Y. Zhang, S.R. Yu, *Fatigue Fract. Eng. Mater. Struct.* 37 (2014) 1146–1152.
- [3] J.Q. Yang, Y. Liu, Z.Y. Ye, D.Z. Yang, S.Y. He, *Surf. Coat. Technol.* 204 (2009) 705–712.
- [4] J.Q. Yang, Y. Liu, Z.Y. Ye, D.Z. Yang, S.Y. He, *Mater. Des.* 32 (2011) 808–814.
- [5] T.M. Shao, M. Hua, H.Y. Tam, *Wear* 255 (2003) 444–455.
- [6] L.N. Tang, M.F. Yan, *Surf. Coat. Technol.* 206 (2012) 2363–2370.
- [7] L.M. Wang, Q. Lin, L.J. Yue, L. Liu, F. Guo, F.M. Wang, *J. Alloy. Compd.* 451 (2008) 534–537.
- [8] C.J. Liu, Y.H. Huang, M.F. Jiang, *J. Iron Steel Res. Int.* 18 (2011) No. 3, 52–58.
- [9] H.H. Yan, Y. Hu, D.W. Zhao, Y.T. Li, *Rare Earths* 46 (2017) 1912–1919.
- [10] Z.Z. Zhang, Y.X. Huang, Y.B. Yan, F. Cao, G. Chen, *Chinese Rare Earths* 22 (2001) No. 4, 56–59.
- [11] H. Liu, D.H. Zheng, Z.Y. Xu, *Ordnance Material and Science Engineering* 15 (1992) No. 3, 8–13.
- [12] W. Lu, D.H. Zheng, Z.Y. Xu, *Acta Metall. Sin.* 29 (1993) A307–A311.
- [13] Z.C. Liu, *Austenite formation and pearlite transformation*, Metallurgical Industry Press, Beijing, China, 2010.
- [14] X.Z. Gao, J.C. Yang, X. Liu, *Sci-Tech Information Development & Economy* 17 (2007) No. 18, 150–152.
- [15] L.J. Yue, *The research of behavior and effect and mechanism of rare earths in Cu-P-RE weathering steel*, Northeastern University, Shenyang, China, 2006.
- [16] T. Du, *J. Iron Steel Res.* 6 (1994) No.3, 6–12.
- [17] L. Chen, X.C. Ma, L.M. Wang, X.N. Ye, *Mater. Des.* 32 (2011) 2206–2212.
- [18] X. Qi, H.H. Mao, Y.T. Yang, *Corros. Sci.* 120 (2017) 90–98.
- [19] S.Y. Lu, K.F. Yao, Y.B. Chen, M.H. Wang, S. Yang, X.Y. Ge, *J. Appl. Electrochem.* 45 (2015) 375–383.
- [20] S.T. Kim, S.H. Jeon, I.S. Lee, Y.S. Park, *Corros. Sci.* 52 (2010) 1897–1904.
- [21] S.H. Jeon, S.T. Kim, M.S. Choi, J.S. Kim, K.T. Kim, Y.S. Park, *Corros. Sci.* 75 (2013) 367–375.
- [22] S.H. Jeon, D.H. Hur, H.J. Kim, Y.S. Park, *Corros. Sci.* 90 (2015) 313–322.